












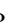



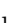




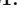




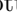




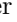









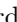







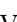


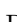



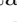
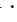
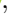



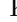





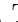

















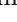
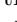

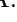
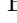

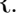

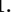

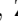


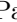




















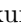



## Evidence of the $P_{c\bar{c}s}(4459)^0$ in $\Upsilon(1S, 2S)$ inclusive decays at Belle

I. Adachi , L. Aggarwal , H. Ahmed , J. K. Ahn , H. Aihara , N. Akopov , M. Alhakami , A. Aloisio , N. Alhubiti , D. M. Asner , H. Atmacan , V. Aushev , M. Aversano , R. Ayad , V. Babu , H. Bae , N. K. Baghel , S. Bahinipati , P. Bambade , Sw. Banerjee , S. Bansal , M. Barrett , M. Bartl , J. Baudot , A. Baur , A. Beaubien , F. Becherer , J. Becker , J. V. Bennett , F. U. Bernlochner , V. Bertacchi , M. Bertemes , E. Bertholet , M. Bessner , S. Bettarini , V. Bhardwaj , B. Bhuyan , F. Bianchi , D. Biswas , D. Bodrov , A. Bolz , A. Boschetti , A. Bozek , M. Bračko , P. Branchini , R. A. Briere , T. E. Browder , A. Budano , S. Bussino , Q. Campagna , M. Campajola , L. Cao , G. Casarosa , C. Cecchi

, J. Cerasoli , M.-C. Chang , P. Chang , R. Cheaib , P. Cheema , B. G. Cheon , K. Chilikin , K. Chirapatpimol , H.-E. Cho , K. Cho , S.-J. Cho , S.-K. Choi , S. Choudhury , J. Cochran , L. Corona , J. X. Cui , E. De La Cruz-Burelo , S. A. De La Motte , G. De Nardo , G. De Pietro , R. de Sangro , M. Destefanis , S. Dey , R. Dhamija , F. Di Capua , J. Dingfelder , Z. Doležal , I. Domínguez Jiménez , T. V. Dong , X. Dong , D. Dossett , K. Dugic , G. Dujany , P. Ecker , J. Eppelt , P. Feichtinger , T. Ferber , T. Fillinger , C. Finck , G. Finocchiaro , F. Forti , B. G. Fulsom , A. Gabrielli , E. Ganiev , M. Garcia-Hernandez , G. Gaudino , V. Gaur , A. Gellrich , G. Ghevondyan , D. Ghosh , H. Ghumaryan , G. Giakoustidis , R. Giordano

, A. Giri , P. Gironella Gironell , A. Glazov , B. Gobbo , R. Godang , P. Goldenzweig , E. Graziani , D. Greenwald , Z. Gruberová , Y. Guan , K. Gudkova , I. Haide , Y. Han , C. Harris , K. Hayasaka , H. Hayashii , S. Hazra , C. Hearty , M. T. Hedges , A. Heidelberg , I. Heredia de la Cruz , M. Hernández Villanueva , T. Higuchi , M. Hoek , M. Hohmann , R. Hoppe , P. Horak , C.-L. Hsu , T. Humair , T. Iijima , K. Inami , N. Ipsita , A. Ishikawa , R. Itoh , M. Iwasaki , P. Jackson , D. Jacobi , W. W. Jacobs , E.-J. Jang , Q. P. Ji , S. Jia , Y. Jin , A. Johnson , K. K. Joo , H. Junkerkalefeld , M. Kaleta , J. Kandra , K. H. Kang , S. Kang , G. Karyan , T. Kawasaki , F. Keil , C. Ketter , C. Kiesling

, C.-H. Kim , D. Y. Kim , J.-Y. Kim , K.-H. Kim , Y.-K. Kim , H. Kindo , K. Kinoshita , P. Kodyš , T. Koga , S. Kohani , K. Kojima , A. Korobov , S. Korpar , E. Kovalenko , P. Križan , P. Krokovny , T. Kuhr , Y. Kulii , D. Kumar , R. Kumar , K. Kumara , T. Kunigo , A. Kuzmin , Y.-J. Kwon , S. Lacaprara , K. Lalwani , T. Lam , J. S. Lange , T. S. Lau , M. Laurenza , R. Lebourder , F. R. Le Diberder , M. J. Lee , C. Lemettais , P. Leo , P. M. Lewis , C. Li , L. K. Li , Q. M. Li , W. Z. Li , Y. Li , Y. B. Li , Y. P. Liao , J. Libby , J. Lin , M. H. Liu , Q. Y. Liu , Y. Liu , Z. Q. Liu , D. Liventsev , S. Longo , C. Lyu , Y. Ma , C. Madaan

, M. Maggiora , S. P. Maharana , R. Maiti , G. Mancinelli , R. Manfredi , E. Manoni , M. Mantovano , D. Marcantonio , S. Marcello , C. Marinas , C. Martellini , A. Martens , A. Martini , T. Martinov , L. Massaccesi , M. Masuda , D. Matvienko , S. K. Maurya , M. Maushart , J. A. McKenna , R. Mehta , F. Meier , D. Meleshko , M. Merola , C. Miller , M. Mirra , S. Mitra , K. Miyabayashi , H. Miyake , R. Mizuk , G. B. Mohanty , S. Mondal , S. Moneta , H.-G. Moser , R. Mussa , I. Nakamura , M. Nakao , H. Nakazawa , Y. Nakazawa , M. Naruki , Z. Natkaniec , A. Natochii , M. Nayak , G. Nazaryan , M. Neu , S. Nishida , S. Ogawa , H. Ono , Y. Onuki , F. Otani , G. Pakhlova , S. Pardi , K. Parham , H. Park

, J. Park , K. Park , S.-H. Park , B. Paschen , S. Patra , T. K. Pedlar , I. Peruzzi , R. Peschke , R. Pestotnik , M. Piccolo , L. E. Piilonen , P. L. M. Podesta-Lerma , T. Podobnik , S. Pokharel , C. Praz , S. Prell , E. Principe , M. T. Prim , H. Purwar , P. Rados , G. Raeuber , S. Raiz , N. Rauls , K. Ravindran , J. U. Rehman , M. Reif , S. Reiter , M. Remnev , L. Reuter , D. Ricalde Herrmann , I. Ripp-Baudot , G. Rizzo , M. Roehrken , J. M. Roney , A. Rostomyan , N. Rout , D. A. Sanders , S. Sandilya , L. Santelj , V. Savinov , B. Scavino , J. Schmitz , S. Schneider , G. Schnell , C. Schwanda , Y. Seino , A. Selce , K. Senyo , J. Serrano , M. E. Sevir , C. Sfienti , W. Shan , C. Sharma , X. D. Shi

, T. Shillington , T. Shimasaki , J.-G. Shiu , D. Shtol , A. Sibidanov , F. Simon , J. B. Singh , J. Skorupa , M. Sobotzik , A. Soffer , A. Sokolov , E. Solovieva , S. Spataro , B. Spruck , W. Song , M. Starič , P. Stavroulakis , S. Stefkova , R. Stroili , J. Strube , Y. Sue , M. Sumihama , K. Sumisawa , W. Sutcliffe , N. Suwonjandee , H. Svidras , M. Takahashi , M. Takizawa , U. Tamponi , K. Tanida , F. Tenchini , A. Thaller , O. Tittel 

R. Tiwary , E. Torassa , K. Trabelsi , I. Tsaklidis , M. Uchida , I. Ueda , K. Unger , Y. Unno , K. Uno ,  
 S. Uno , P. Urquijo , Y. Ushiroda , S. E. Vahsen , R. van Tonder , M. Veronesi , A. Vinokurova ,  
 V. S. Vismaya , L. Vitale , V. Vobbiliseti , R. Volpe , A. Vossen , M. Wakai , S. Wallner , M.-Z. Wang ,  
 X. L. Wang , Z. Wang , A. Warburton , M. Watanabe , S. Watanuki , C. Wessel , E. Won , X. P. Xu ,  
 B. D. Yabsley , S. Yamada , S. B. Yang , J. Yelton , J. H. Yin , K. Yoshihara , C. Z. Yuan , J. Yuan ,  
 L. Zani , F. Zeng , B. Zhang , J. S. Zhou , Q. D. Zhou , L. Zhu , V. I. Zhukova , R. Žlebčík , and S. Zou 

(The Belle and Belle II Collaborations)

Using data samples of 102 million  $\Upsilon(1S)$  events and 158 million  $\Upsilon(2S)$  events collected by the Belle detector at the KEKB asymmetric-energy  $e^+e^-$  collider, we search for  $[udsc\bar{c}]$  pentaquark states decaying to  $J/\psi\Lambda$ . Using the first observations of  $\Upsilon(1S, 2S)$  inclusive decays to  $J/\psi\Lambda$ , we find evidence of the  $P_{c\bar{c}s}(4459)^0$  state with a significance of 3.3 standard deviations, including statistical and systematic uncertainties. We measure the mass and width of the  $P_{c\bar{c}s}(4459)^0$  to be  $(4471.7 \pm 4.8 \pm 0.6)$  MeV/ $c^2$  and  $(21.9 \pm 13.1 \pm 2.7)$  MeV, respectively. The branching fractions for  $P_{c\bar{c}s}(4459)^0$  production are measured to be  $\mathcal{B}[\Upsilon(1S) \rightarrow P_{c\bar{c}s}(4459)^0/\bar{P}_{c\bar{c}s}(4459)^0 + \text{anything}] = (3.5 \pm 2.0 \pm 0.2) \times 10^{-6}$  and  $\mathcal{B}[\Upsilon(2S) \rightarrow P_{c\bar{c}s}(4459)^0/\bar{P}_{c\bar{c}s}(4459)^0 + \text{anything}] = (2.9 \pm 1.7 \pm 0.4) \times 10^{-6}$ . The inclusive branching fractions of  $\Upsilon(1S, 2S) \rightarrow J/\psi\Lambda/\bar{\Lambda}$  are measured to be  $\mathcal{B}[\Upsilon(1S) \rightarrow J/\psi\Lambda/\bar{\Lambda} + \text{anything}] = (36.9 \pm 5.3 \pm 2.4) \times 10^{-6}$  and  $\mathcal{B}[\Upsilon(2S) \rightarrow J/\psi\Lambda/\bar{\Lambda} + \text{anything}] = (22.3 \pm 5.7 \pm 3.1) \times 10^{-6}$ . We measure the visible cross section  $\sigma(e^+e^- \rightarrow J/\psi\Lambda/\bar{\Lambda} + \text{anything}) = (90 \pm 14 \pm 6)$  fb for the continuum production at  $\sqrt{s} = 10.52$  GeV. In all cases, the first uncertainties are statistical and the second are systematic.

Interest in pentaquark states started in the 1960's as both Gell-Mann and Zweig postulated their existence in their first descriptions of the quark model [1, 2]. The first observation of the charged pentaquark state candidates,  $P_{cc}^+$ , with valence quark content  $[uudc\bar{c}]$  was reported in the decay  $\Lambda_b \rightarrow J/\psi p K^-$  by the LHCb experiment [3, 4]. In a subsequent search for a neutral pentaquark, LHCb reported evidence ( $3.1\sigma$ ) of a pentaquark candidate state with a suggested quark assignment  $[udsc\bar{c}]$  [5], named the  $P_{c\bar{c}s}(4459)^0$  with a mass of  $(4458.8 \pm 2.9_{-1.1}^{+4.7})$  MeV/ $c^2$  and a width of  $(17.3 \pm 6.5_{-5.7}^{+8.0})$  MeV, in the  $J/\psi\Lambda$  substructure of the decay  $\Xi_b^- \rightarrow J/\psi\Lambda K^-$  [6]. Here and hereinafter, the first uncertainty quoted is statistical, and the second is systematic. Another candidate  $P_{c\bar{c}s}(4338)^0$ , sharing the same suggested valence quark content, was discovered in the decay of  $B^- \rightarrow J/\psi\Lambda\bar{p}$  [7] with a statistical significance exceeding  $15\sigma$ , a measured mass of  $(4338.2 \pm 0.7 \pm 0.4)$  MeV/ $c^2$ , and a width of  $(7.0 \pm 1.2 \pm 1.3)$  MeV.

The pentaquark candidates found by LHCb are all at masses close to the production thresholds of ordinary baryon-meson states, i.e.,  $\Sigma_c^+ \bar{D}^{(*)0}$  for the  $P_{cc}^+$  states [3, 4],  $\Xi_c^0 \bar{D}^{*0}$  for the  $P_{c\bar{c}s}(4459)^0$  state [6] and  $\Xi_c^+ D^-$  for the  $P_{c\bar{c}s}(4338)^0$  state [7]. There are various interpretations of these states, including tightly-bound pentaquark states [8, 9], loosely-bound baryon-meson molecular states [10, 11], or the product of rescattering effects [12]. However, their nature is still largely unknown and further investigation is needed. Moreover, these states have so far only been reported by LHCb, and it is essential to provide independent confirmation of their existence.

Theoretical considerations suggest that  $\Upsilon(1S)$  and  $\Upsilon(2S)$  decays could produce final states of matter with

unusual quark configurations, such as  $qq\bar{q}\bar{q}$  or  $qqq\bar{q}\bar{q}$  [13]. Meanwhile, the observations of inclusive production of the antideuteron, a candidate for a hexaquark bound system [14], by the ARGUS, CLEO, and BaBar experiments in  $\Upsilon(1S)$  and  $\Upsilon(2S)$  inclusive decays [15–17], suggest searching for a  $P_{cc}^+$  or  $P_{c\bar{c}s}^0$  state in the same data sample. In a study of the  $pJ/\psi$  final state from  $\Upsilon(1S, 2S)$  inclusive decays [18], Belle saw no significant  $P_{cc}^+$  signal. However, this work did report a branching fraction  $\mathcal{B}[\Upsilon(1S, 2S) \rightarrow J/\psi p/\bar{p} + \text{anything}]$  at the  $10^{-5}$  level.

This Letter reports the results of a search for  $P_{c\bar{c}s}^0$  states in the  $J/\psi\Lambda$  final state of  $\Upsilon(1S, 2S)$  inclusive decays using the world's largest  $\Upsilon(1S)$  and  $\Upsilon(2S)$  data samples, produced by the KEKB collider [19, 20] and collected by the Belle detector [21]. Here, the  $J/\psi$  is reconstructed in the  $\ell^+\ell^-$  ( $\ell = e, \mu$ ) final state and  $\Lambda$  in its decay to  $p\pi^-$ . Inclusion of charge-conjugate processes is implied. The  $\Upsilon(1S)$  data sample has an integrated luminosity of  $\mathcal{L}_{\Upsilon(1S)} = 5.8$  fb $^{-1}$  and  $(1.02 \pm 0.02) \times 10^8$   $\Upsilon(1S)$  events [22], and the  $\Upsilon(2S)$  data sample has  $\mathcal{L}_{\Upsilon(2S)} = 24.5$  fb $^{-1}$  and  $(1.58 \pm 0.04) \times 10^8$   $\Upsilon(2S)$  events [23]. As  $\Upsilon(1S, 2S)$  are produced from  $e^+e^-$  annihilation, a data sample collected at  $\sqrt{s} = 10.52$  GeV with an integrated luminosity of  $\mathcal{L}_{\text{cont}} = 89$  fb $^{-1}$  (referred to as the ‘‘continuum data sample’’) is used to study  $J/\psi\Lambda$  production.

To optimize the signal selection criteria and determine the reconstruction efficiencies and resolutions, we use EvtGen [24] to simulate the signal Monte Carlo (MC) samples of  $\Upsilon(1S, 2S) \rightarrow P_{c\bar{c}s}^0 \bar{\Lambda} + q\bar{q}$  with  $P_{c\bar{c}s}^0 \rightarrow J/\psi\Lambda$  based on phase space [24]; Here,  $P_{c\bar{c}s}^0$  represents  $P_{c\bar{c}s}(4459)^0$  or  $P_{c\bar{c}s}(4338)^0$ , and  $q\bar{q}$  ( $q = u, d, s, c$ ) denotes a quark-antiquark pair whose hadronization is simulated using PYTHIA [25]. To investigate the efficiency and the resolution dependence on the  $J/\psi\Lambda$  invariant mass

( $M_{J/\psi\Lambda}$ ), we generate a range of signal MC samples with  $M_{J/\psi\Lambda}$  varying from 4.3  $\text{GeV}/c^2$  to 5.6  $\text{GeV}/c^2$  and an intrinsic width set to zero. To examine non-resonant  $J/\psi\Lambda$ , we generate MC samples of  $\Upsilon(1S, 2S) \rightarrow J/\psi\Lambda\bar{p}K^+ + q\bar{q}$  using phase space [24] and these are referred to as the “no- $P_{ccs}^0$  MC samples”. The  $q\bar{q}$  system in the  $\Upsilon(1S)$  [ $\Upsilon(2S)$ ] decays is generated with a mass of 2.6  $\text{GeV}/c^2$  (3.2  $\text{GeV}/c^2$ ) and a broad width of 1.7 GeV. We employ a GEANT3-based MC technique [26] to simulate the response of the Belle detector. We use the Belle II analysis software framework (basf2) [27] to reconstruct the events for Belle data. The Belle data is converted to the Belle II format for basf2 compatibility using the B2BII software package [28].

The charged tracks, except for those used in the reconstruction of  $\Lambda$  candidates, are selected to originate from the interaction point by requiring their impact parameters to be less than 2.0 cm along the beam direction ( $dz$ ), and less than 0.2 cm in the transverse plane ( $dr$ ). Two tracks with opposite charges and a difference of  $dz$  less than 0.2 cm are selected as candidates of the lepton pair from  $J/\psi$  decay. Electrons are identified by having  $\mathcal{L}_e/(\mathcal{L}_e + \mathcal{L}_h) > 0.9$ , where the electron likelihood  $\mathcal{L}_e$  and hadron likelihood  $\mathcal{L}_h$  ( $h = \pi, K, p$ ) are assigned based on central drift chamber, aerogel threshold Cherenkov counter, and electromagnetic calorimeter (ECL) information [29, 30]. Tracks are identified as muons if they have  $\mathcal{L}_\mu/(\mathcal{L}_\mu + \mathcal{L}_\pi + \mathcal{L}_K) > 0.9$ , where the muon likelihood  $\mathcal{L}_\mu$  is assigned based on the range and hit positions of the extrapolated track in the  $K_L$  and muon detector [31]. The particle identification (PID) efficiency of a single lepton is  $(93.9 \pm 0.2)\%$  for  $e^\pm$  and  $(91.9 \pm 0.2)\%$  for  $\mu^\pm$ . Bremsstrahlung photons detected in the ECL within a cone of 0.05 radians about the original  $e^\pm$  direction are incorporated into the calculation of the  $e^+e^-$  ( $\gamma$ ) invariant mass. The  $\Lambda$  candidates are reconstructed in the  $\Lambda \rightarrow p\pi^-$  decay mode using an artificial neural network [32], which uses vertex fit and the PID information,  $\mathcal{L}_p/(\mathcal{L}_p + \mathcal{L}_\pi)$ , to identify  $p$  and  $\pi^-$  candidates.

Figure 1 shows scatter plots of the invariant mass of the lepton pair ( $M_{\ell^+\ell^-}$ ) versus the  $p\pi^-$  pair ( $M_{p\pi^-}$ ) from the  $\Upsilon(1S, 2S)$  data samples. Clear  $J/\psi$  and  $\Lambda$  signals are visible. By fitting the  $M_{\ell^+\ell^-}$  distribution with a double Gaussian function for the  $J/\psi$  signals and a first-order Chebychev function for the backgrounds, we obtain the resolutions  $\sigma_{J/\psi}^{\text{data}} = 9.4 \pm 0.1 \text{ MeV}/c^2$  in data and  $\sigma_{J/\psi}^{\text{MC}} = 9.2 \pm 0.1 \text{ MeV}/c^2$  in signal MC simulation. Similarly, we obtain  $\sigma_\Lambda^{\text{data}} = 1.4 \pm 0.2 \text{ MeV}/c^2$  and  $\sigma_\Lambda^{\text{MC}} = 1.3 \pm 0.1 \text{ MeV}/c^2$  for the  $\Lambda$  signals by fitting to the  $M_{p\pi^-}$  distributions in data and signal MC simulation. We define the signal regions as  $|M_{\ell^+\ell^-} - m_{J/\psi}| < 30 \text{ MeV}/c^2$  and  $|M_{p\pi^-} - m_\Lambda| < 4.2 \text{ MeV}/c^2$ , where  $m_{J/\psi}$  and  $m_\Lambda$  are the nominal masses of the  $J/\psi$  and  $\Lambda$  [33]. The central red boxes in Fig. 1 show the signal regions. To estimate the backgrounds in the  $\Lambda$

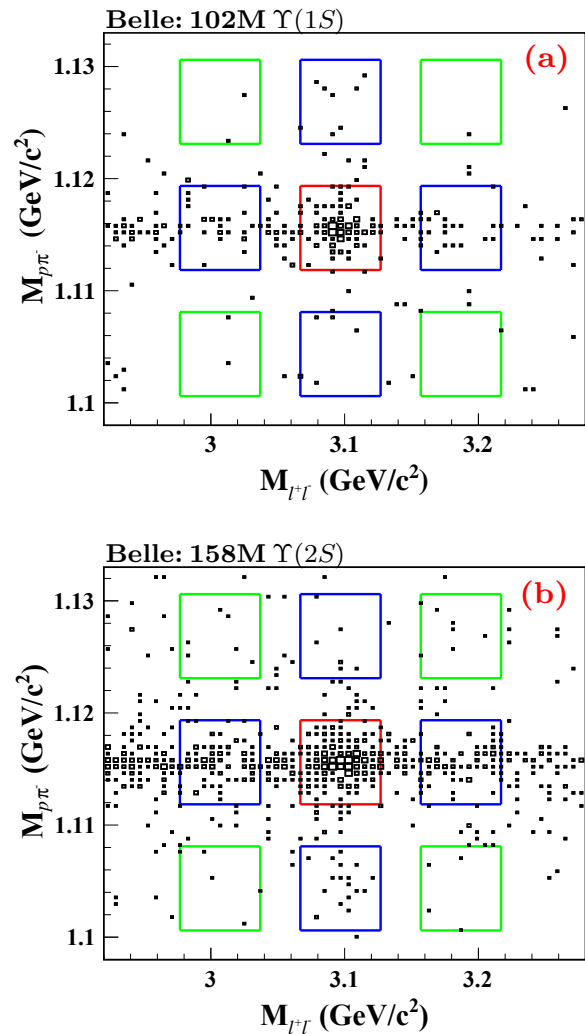


FIG. 1. Two-dimensional scatter plots of  $M_{\ell^+\ell^-}$  versus  $M_{p\pi^-}$  from (a) the  $\Upsilon(1S)$  data sample and (b) the  $\Upsilon(2S)$  data sample. The central red boxes are the signal regions, while the blue and green boxes around it are the two-dimensional sideband regions.

and  $J/\psi$  reconstructions, we define one-dimensional sideband regions as  $|M_{\ell^+\ell^-} - m_{J/\psi} \pm 90| < 30 \text{ MeV}/c^2$  and  $|M_{p\pi^-} - m_\Lambda \pm 12.6| < 4.2 \text{ MeV}/c^2$ . Combining these one-dimensional mass ranges, we define two-dimensional sideband regions shown by the rectangles in Fig. 1 which surround the signal area. With  $N_{B_1}$  ( $N_{B_2}$ ) representing the sum of the events in the four sideband regions nearest (diagonal to) the signal region, the yield of backgrounds to the reconstructed  $\Lambda$  and  $J/\psi$  candidates are calculated to be  $N_B = 0.5N_{B_1} - 0.25N_{B_2}$ .

After subtracting the backgrounds estimated from the two-dimensional sidebands, the numbers of  $J/\psi\Lambda$  candidates in the signal regions are  $N_{\Upsilon(1S)}^{J/\psi\Lambda} = 84 \pm 11$ ,  $N_{\Upsilon(2S)}^{J/\psi\Lambda} = 140 \pm 17$ , and  $N_{\text{cont}}^{J/\psi\Lambda} = 134 \pm 21$  in the  $\Upsilon(1S)$ ,  $\Upsilon(2S)$ , and continuum data samples, respectively. According to the no- $P_{ccs}^0$  MC simulations, their efficiencies

are  $\varepsilon_{\Upsilon(1S)} = (26.5 \pm 0.2)\%$  and  $\varepsilon_{\Upsilon(2S)} = (27.0 \pm 0.2)\%$  in  $\Upsilon(1S)$  and  $\Upsilon(2S)$  inclusive decays, and  $\varepsilon_{\text{cont}} = (26.6 \pm 0.2)\%$  in the  $e^+e^-$  annihilation. To estimate the continuum background in the  $\Upsilon(1S, 2S)$  data samples from the continuum data sample, we scale the luminosity and correct for the energy dependence of the cross section assuming  $\sigma_{e^+e^-} \propto 1/s$ , and this results in a scale factor  $f_{\text{scale}} = [\mathcal{L}_{\Upsilon(1S,2S)}\varepsilon_{\Upsilon(1S,2S)}s_{\text{cont}}]/[\mathcal{L}_{\text{cont}}\varepsilon_{\text{cont}}s_{\Upsilon(1S,2S)}] = 0.058$  and  $0.266$  for the  $\Upsilon(1S)$  and  $\Upsilon(2S)$  data samples, respectively.

We measure the cross section of the inclusive production of  $J/\psi \Lambda/\bar{\Lambda}$  in  $e^+e^-$  annihilation via the equation

$$\sigma(e^+e^- \rightarrow J/\psi \Lambda/\bar{\Lambda} + \text{anything}) = \frac{N_{\text{cont}}^{J/\psi\Lambda}}{\mathcal{L}_{\text{cont}}\varepsilon_{\text{cont}}\mathcal{B}(J/\psi \rightarrow \ell^+\ell^-)\mathcal{B}(\Lambda \rightarrow p\pi^-)(1 + \delta_{\text{ISR}})}, \quad (1)$$

where  $\mathcal{B}(J/\psi \rightarrow \ell^+\ell^-)$  and  $\mathcal{B}(\Lambda \rightarrow p\pi^-)$  are the world average values of the branching fractions of  $J/\psi$  and  $\Lambda$  decays [33], and the radiative correction factor  $1 + \delta_{\text{ISR}}$  is calculated to be 0.82 [34, 35]. We obtain  $\sigma(e^+e^- \rightarrow J/\psi \Lambda/\bar{\Lambda} + \text{anything}) = (90 \pm 14 \pm 6)$  fb at  $\sqrt{s} = 10.52$  GeV, where the systematic uncertainties will be described below.

We then measure the production of  $J/\psi \Lambda/\bar{\Lambda}$  in  $\Upsilon(1S, 2S)$  inclusive decays. We calculate the branching fractions of  $\Upsilon(1S)$  inclusive decays to  $J/\psi \Lambda/\bar{\Lambda}$  using

$$\mathcal{B}[\Upsilon(1S) \rightarrow J/\psi \Lambda/\bar{\Lambda} + \text{anything}] = \frac{N_{\Upsilon(1S)}^{J/\psi\Lambda} - f_{\text{scale}}N_{\text{cont}}^{J/\psi\Lambda}}{N_{\Upsilon(1S)}\varepsilon_{\Upsilon(1S)}\mathcal{B}(J/\psi \rightarrow \ell^+\ell^-)\mathcal{B}(\Lambda \rightarrow p\pi^-)}, \quad (2)$$

and find a value  $(36.9 \pm 5.3 \pm 2.4) \times 10^{-6}$ . Similarly, we obtain  $\mathcal{B}[\Upsilon(2S) \rightarrow J/\psi \Lambda/\bar{\Lambda} + \text{anything}] = (32.0 \pm 5.5 \pm 3.0) \times 10^{-6}$ . Subtracting the contribution due to  $\Upsilon(2S)$  to  $\Upsilon(1S)$  transitions [33], we find the branching fraction for direct  $\Upsilon(2S)$  inclusive decays to be  $\mathcal{B}[\Upsilon(2S) \rightarrow J/\psi \Lambda/\bar{\Lambda} + \text{anything}] = (22.3 \pm 5.7 \pm 3.1) \times 10^{-6}$ . These are the first measurements of these inclusive branching fractions.

The  $M_{J/\psi\Lambda}$  distributions from 4.2 GeV/ $c^2$  to 4.7 GeV/ $c^2$  in the  $\Upsilon(1S)$ ,  $\Upsilon(2S)$  and continuum data samples are illustrated in Fig. 2. To avoid the broadening due to the mass resolutions of the  $\ell^+\ell^-$  and  $p\pi^-$  combinations, we use the calculation  $M_{J/\psi\Lambda} = M_{\ell^+\ell^-p\pi^-} - M_{\ell^+\ell^-} - M_{p\pi^-} + m_{J/\psi} + m_{\Lambda}$ , where  $M_{\ell^+\ell^-p\pi^-}$  is the invariant mass calculated from the sum of the 4-momenta of the  $\ell^+\ell^-$  and  $p\pi^-$  pairs. Using this procedure improves the resolution in the  $M_{J/\psi\Lambda}$  distribution from the signal MC to 2.2 MeV/ $c^2$  for  $P_{c\bar{c}s}(4338)^0$  and 2.8 MeV/ $c^2$  for  $P_{c\bar{c}s}(4459)^0$ , compared to about 11.5 MeV/ $c^2$  and 12.3 MeV/ $c^2$  in the  $M_{\ell^+\ell^-p\pi^-}$  distribution. There are event accumulations near the mass of  $P_{c\bar{c}s}(4459)^0$  in the  $\Upsilon(1S)$  and  $\Upsilon(2S)$  data samples, but none in the  $P_{c\bar{c}s}(4338)^0$  region.

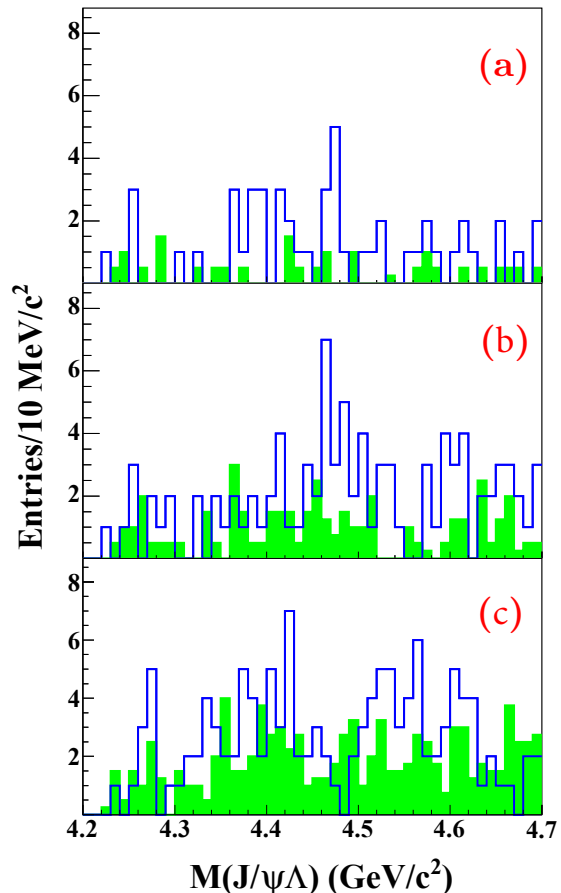


FIG. 2. The invariant mass distributions of  $J/\psi\Lambda$  from (a) the  $\Upsilon(1S)$  data sample, (b) the  $\Upsilon(2S)$  data sample, and (c) the continuum data sample. The open blue blank histograms show the events in signal regions, while the green histograms show the background estimated from the two-dimensional sideband regions.

A binned maximum-likelihood fit is performed to the  $J/\psi\Lambda$  mass spectrum obtained from the combined  $\Upsilon(1S, 2S)$  data sample to study the excess, and this is shown in Fig. 3. The fit is performed with a bin width of 1 MeV/ $c^2$  rather than the 10 MeV/ $c^2$  used in the figure for display purposes. The probability density function (PDF) used to describe the events selected from the signal region is characterized by

$$f_{\text{PDF}} = f_{\text{R}} + f_{\text{noPcs}} + f_{\text{SB}}, \quad (3)$$

where  $f_{\text{R}}$  is for the resonance,  $f_{\text{SB}}$  is the background estimated from the two-dimensional sidebands, and  $f_{\text{noPcs}}$  is for the no- $P_{c\bar{c}s}^0$  production. Here,  $f_{\text{R}}$  is the convolution of a Breit-Wigner function and a Gaussian function with the resolution fixed to the value of 2.8 MeV/ $c^2$  obtained from the signal MC simulation. We use  $\sqrt{M_{J/\psi\Lambda} - M_{\text{thr}}} \times e^{c_0 M_{J/\psi\Lambda}}$  for  $f_{\text{SB}}$ , where  $M_{\text{thr}} = 4.21$  GeV/ $c^2$  is the mass

threshold of  $J/\psi\Lambda$ , and  $c_0$  is a coefficient determined by the fit.  $f_{\text{no}P_{c\bar{c}s}}$  is the histogram PDF of  $M_{J/\psi\Lambda}$  obtained from the no- $P_{c\bar{c}s}^0$  MC simulation. We fit simultaneously to the events from the signal region with  $f_{\text{PDF}}$  and events from the two-dimensional sideband regions with  $f_{\text{SB}}$ . The likelihood for the fit is denoted as  $\mathcal{L}$ .

Since the excess is close to the mass of  $P_{c\bar{c}s}(4459)^0$ , we include a Gaussian constraint using prior knowledge of the LHCb measurement [6] in the fit and minimize the value of

$$-2 \ln \mathcal{L}' \equiv -2 \ln \mathcal{L} + \frac{(m - m_0)^2}{\sigma_{m_0}^2} + \frac{(\Gamma - \Gamma_0)^2}{\sigma_{\Gamma_0}^2}, \quad (4)$$

where  $m$  and  $\Gamma$  are the mass and width of the signal structure,  $m_0$  and  $\Gamma_0$  are the mean values from the LHCb's measurement [6], and  $\sigma_{m_0}$  and  $\sigma_{\Gamma_0}$  represent their asymmetric uncertainties. If the values of masses or widths from the fits are greater than LHCb's measurements, positive uncertainties are quoted; otherwise, negative uncertainties are used. The fit yields the number of  $P_{c\bar{c}s}(4459)^0$  signal events  $N_{P_{c\bar{c}s}(4459)^0} = 21 \pm 5$ . By removing the  $f_R$  term from  $f_{\text{PDF}}$  in Eq. (3), i.e., if we use the background-only hypothesis, the new fit yields a change  $\Delta(-2 \ln \mathcal{L}') = 13.01$ . The significance of the signal is estimated using a pseudo-experiment technique. The pseudo-experiments are generated based on the fit result of the background-only hypothesis, assuming a Poisson distribution of events in each bin of the  $M_{J/\psi\Lambda}$  distribution. The fit in each pseudo-experiment follows the same procedures as in the nominal fit. Among the  $4.3 \times 10^5$  pseudo-experiments, only 160 have  $\Delta(-2 \ln \mathcal{L}') > 13.01$ . This corresponds to a  $p$ -value of  $3.8 \times 10^{-4}$  and thus a significance of  $3.4\sigma$  for the  $P_{c\bar{c}s}(4459)^0$  in the combined  $\Upsilon(1S, 2S)$  data sample. To estimate the systematic uncertainty due to the background modeling, we replace the exponential function in  $f_{\text{SB}}$  with a second-order Chebyshev function. This results in a significance for the  $P_{c\bar{c}s}(4459)^0$  of  $3.3\sigma$  including systematic uncertainties.

We also perform a fit without the mass and width constraints. The fit yields a mass of  $M_R = (4471.7 \pm 4.8 \pm 0.6) \text{ MeV}/c^2$  and a width of  $\Gamma_R = (21.9 \pm 13.1 \pm 2.7) \text{ MeV}$  for this structure, where the systematic uncertainties are described below. The fit results agree with the measurements for the  $P_{c\bar{c}s}(4459)^0$  as reported by LHCb at a significance of  $1.8\sigma$  in mass and  $0.3\sigma$  in width. The local significance is calculated to be  $3.8\sigma$  according to  $\Delta(-2 \ln \mathcal{L}) = 14.58$ .

We also calculate the branching fraction for  $P_{c\bar{c}s}^0$  production in the  $\Upsilon(1S, 2S)$  inclusive decays by

$$\mathcal{B}[\Upsilon(1S, 2S) \rightarrow P_{c\bar{c}s}^0 / \bar{P}_{c\bar{c}s}^0 + \text{anything}] \mathcal{B}(P_{c\bar{c}s}^0 \rightarrow J/\psi\Lambda) = \frac{N_{P_{c\bar{c}s}^0}^{\text{fit}}}{N_{\Upsilon(1S, 2S)} \varepsilon_{P_{c\bar{c}s}^0} \mathcal{B}(J/\psi \rightarrow \ell^+ \ell^-) \mathcal{B}(\Lambda \rightarrow p\pi^-)}, \quad (5)$$

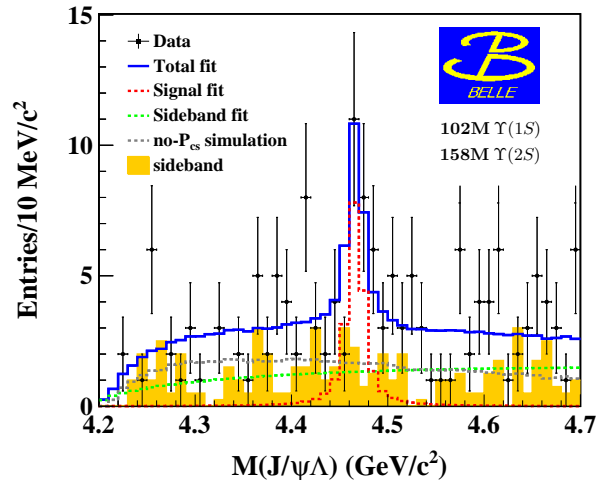


FIG. 3. The distribution of the invariant mass of  $J/\psi\Lambda$  in combined  $\Upsilon(1S, 2S)$  data sample and the fit results with mass and width constrained. The points with error bars are the data, and the yellow histogram is the background estimated from the two-dimensional sideband regions. The solid curve shows the best fit results. The red dashed curve shows the signal. The brown dashed curve shows the no- $P_{c\bar{c}s}^0$  component. The green dashed curve shows the fit to the background estimated from the sidebands.

where  $N_{P_{c\bar{c}s}^0}^{\text{fit}}$  is the number of the signal events of  $P_{c\bar{c}s}^0$  in the fit with constraints, and  $\varepsilon_{P_{c\bar{c}s}^0}$  is the corresponding efficiency. Table I shows the results for  $P_{c\bar{c}s}(4459)^0$ . In calculating the branching fraction in  $\Upsilon(2S)$  inclusive decays, the contribution of the transition from  $\Upsilon(2S)$  to  $\Upsilon(1S)$  is removed.

We perform a fit to  $M_{J/\psi\Lambda}$  with both the  $P_{c\bar{c}s}(4459)^0$  and  $P_{c\bar{c}s}(4338)^0$  resonance included in  $f_R$ . This fit uses a histogram PDF obtained from a signal MC simulation of  $P_{c\bar{c}s}(4338)^0$ . Since there is no significant  $P_{c\bar{c}s}(4338)^0$  signal, we calculate the upper limits on the signal yields  $[N_{P_{c\bar{c}s}(4338)^0}^{\text{fit, UL}}]$  at 90% confidence level (C.L.) by solving the equation

$$\int_0^{N_{P_{c\bar{c}s}(4338)^0}^{\text{fit, UL}}} \mathcal{L}(N) dN / \int_0^{+\infty} \mathcal{L}(N) dN = 0.90, \quad (6)$$

where  $N$  is the assumed signal yield, and  $\mathcal{L}(N)$  is the corresponding maximized likelihood from the fit. To take into account the systematic uncertainties discussed below, the above likelihood is convolved with a Gaussian function whose width equals the total systematic uncertainty. Similarly, we estimate an upper limit for the branching fraction of  $P_{c\bar{c}s}(4338)^0$  produced in  $\Upsilon(1S, 2S)$  inclusive decays at 90% C.L. by replacing  $N_{\text{sig}}^{\text{fit}}$  with  $N_{P_{c\bar{c}s}(4338)^0}^{\text{fit, UL}}$  in Eq. (5). The results are listed in Table I.

Table II summarizes the systematic uncertainties in the determination of the branching fractions and cross section. The uncertainties due to lepton identification are 2.0% for the  $e^+e^-$  mode and 0.5% for the  $\mu^+\mu^-$  mode

TABLE I. The branching fractions and upper limits at 90% C.L. for  $\Upsilon(1S, 2S)$  inclusive decays into  $P_{c\bar{c}s}^0$  with  $P_{c\bar{c}s}^0 \rightarrow J/\psi\Lambda$ .

Mode	$\mathcal{B}(\times 10^{-6})$
$\Upsilon(1S) \rightarrow P_{c\bar{c}s}(4459)^0/\bar{P}_{c\bar{c}s}(4459)^0 + anything$	$3.5 \pm 2.0 \pm 0.2$
$\Upsilon(2S) \rightarrow P_{c\bar{c}s}(4459)^0/\bar{P}_{c\bar{c}s}(4459)^0 + anything$	$2.9 \pm 1.7 \pm 0.4$
$\Upsilon(1S) \rightarrow P_{c\bar{c}s}(4338)^0/\bar{P}_{c\bar{c}s}(4338)^0 + anything$	$< 1.8$
$\Upsilon(2S) \rightarrow P_{c\bar{c}s}(4338)^0/\bar{P}_{c\bar{c}s}(4338)^0 + anything$	$< 1.6$

from  $J/\psi$  decay, contributing 1.4% in total. The uncertainty due to tracking efficiency is 0.35% per track and added linearly. The  $\Lambda$  reconstruction uncertainties are estimated from a  $\Lambda$  sample with a loose selection, and are 4.0% for  $\Upsilon(1S)$  decays, and 3.6% for  $\Upsilon(2S)$  decays, and 3.4% for continuum production, corresponding to the efficiencies difference between data and MC. By fitting to the  $M_{\ell^+\ell^-}$  and  $M_{p\pi^-}$  distributions, we obtain the efficiencies of the mass windows from data ( $\varepsilon^{\text{data}}$ ) and signal MC simulation ( $\varepsilon^{\text{MC}}$ ) in  $\Upsilon(1S, 2S)$  inclusive decays. We take the ratio of  $|\varepsilon_{J/\psi}^{\text{data}} - \varepsilon_{J/\psi}^{\text{MC}}|/\varepsilon_{J/\psi}^{\text{data}}$  as a conservative estimate of the systematic uncertainty, and find 2.1% (1.0%) in  $\Upsilon(1S)$  [ $\Upsilon(2S)$ ] decays, and 2.0% in continuum production for the  $J/\psi$  mass window. Similarly, we obtain 1.6% (3.2%) in  $\Upsilon(1S)$  [ $\Upsilon(2S)$ ] decays, and 2.7% in continuum production for the  $\Lambda$  mass window. The uncertainties of modeling the final states in MC simulations are estimated by varying the mean mass of the  $q\bar{q}$  system to 3.3 GeV/ $c^2$  (2.5 GeV/ $c^2$ ) for  $\Upsilon(1S)$  [ $\Upsilon(2S)$ ] decays. We find that the efficiency changes to be 1.8% in  $\Upsilon(1S)$  decays, 1.7% in  $\Upsilon(2S)$  decays, and 1.8% in continuum production, and take these values as the systematic uncertainties. The uncertainties of the efficiencies of the “no- $P_{c\bar{c}s}^0$  MC samples” are estimated by studying the variations in efficiencies across different MC samples with different accompanying particle, such as  $\Upsilon(1S, 2S) \rightarrow J/\psi\Lambda\bar{\Lambda} + q\bar{q}$  and  $e^+e^- \rightarrow J/\psi\Lambda\bar{\Lambda} + q\bar{q}$ . We take the efficiency differences as the systematic uncertainties, which are 2.3% in  $\Upsilon(1S)$  decay, 3.5% in  $\Upsilon(2S)$  decay, and 1.9% in continuum production. We use the Particle Data Group values [33] for the uncertainties in the branching fractions for  $J/\psi \rightarrow e^+e^-/\mu^+\mu^-$  decays (1.1%),  $\Lambda \rightarrow p\pi^-$  decays (0.8%), and the  $\Upsilon(2S)$  to  $\Upsilon(1S)$  decays (6.1%). The uncertainty in the total numbers of  $\Upsilon(1S)$  [ $\Upsilon(2S)$ ] events in the data sample is 2.0% (2.6%) [22, 23]. The uncertainty in the integrated luminosity of each of the data sample is 1.4% and they are highly correlated, which cancels in the scale factor  $f_{\text{scale}}$ . The statistical uncertainties of the signal MC samples are 0.5% in common. By varying the photon energy cut-off by 50 MeV in the simulation of ISR, we determine the change of  $1+\delta_{\text{ISR}}$  to be 0.01 and take 1.0% to be a conservative systematic uncertainty in the cross section

$\sigma(e^+e^- \rightarrow J/\psi\Lambda/\bar{\Lambda} + anything)$  at  $\sqrt{s} = 10.52$  GeV. We sum the uncertainties in quadrature, assuming they are independent, and obtain total systematic uncertainties of 6.4%, 9.5%, and 6.2% for the measurements of  $\Upsilon(1S)$  decays,  $\Upsilon(2S)$  decays and continuum  $e^+e^-$  annihilation, respectively.

TABLE II. Systematic uncertainties (%) in the  $J/\psi\Lambda/\bar{\Lambda}$  production measurement.

Source	$\Upsilon(1S)$	$\Upsilon(2S)$	$e^+e^-$ annihilation
PID	1.4	1.4	1.4
Tracking	1.4	1.4	1.4
$\Lambda$ selection	4.0	3.6	3.4
$J/\psi$ mass window	2.1	1.0	2.0
$\Lambda$ mass window	1.6	3.2	2.7
Mean mass of $q\bar{q}$ system	1.8	1.7	1.8
Accompanying particle	2.3	3.5	1.9
Branching fractions	1.4	6.3	1.4
$N_{\Upsilon(1S, 2S)}$	2.0	2.6	–
Luminosity	–	–	1.4
MC sample statistics	0.5	0.5	0.5
$1+\delta_{\text{ISR}}$	–	–	1.0
Sum in quadrature	6.4	9.5	6.2

To determine the systematic uncertainties of the resonant parameters of the  $P_{c\bar{c}s}(4459)^0$  structure, we change the following input parameters to the fit. The two-dimensional sidebands are shifted by  $\pm 1\sigma$  in the resolutions. The exponential function in  $f_{\text{SB}}$  is replaced with a second-order Chebyshev function. The bin width is changed from 1 MeV/ $c^2$  to 2 MeV/ $c^2$ . The mass resolution is varied by 10%. The estimation of the systematic uncertainty in modeling the no- $P_{c\bar{c}s}^0$  MC simulation is the same as described previously, and the decay mode  $\Upsilon(1S, 2S) \rightarrow J/\psi\Lambda\bar{\Lambda} + q\bar{q}$  is also taken into account. The differences between the nominal fit results and those from these fits are taken as the systematic uncertainties, which are 0.6 MeV/ $c^2$  for the mass and 2.7 MeV for the width.

In conclusion, using Belle data samples, we report the first observation of  $J/\psi\Lambda$  production in  $\Upsilon(1S, 2S)$  decays and  $e^+e^-$  continuum annihilation. We measure the branching fractions to be  $\mathcal{B}[\Upsilon(1S) \rightarrow J/\psi\Lambda/\bar{\Lambda} + anything] = (36.9 \pm 5.3 \pm 2.4) \times 10^{-6}$  and  $\mathcal{B}[\Upsilon(2S) \rightarrow J/\psi\Lambda/\bar{\Lambda} + anything] = (22.3 \pm 5.7 \pm 3.1) \times 10^{-6}$ , and the cross section to be  $\sigma(e^+e^- \rightarrow J/\psi\Lambda/\bar{\Lambda} + anything) = (90 \pm 14 \pm 6)$  fb at  $\sqrt{s} = 10.52$  GeV. We find a resonance-like peak in the  $J/\psi\Lambda$  invariant mass distribution in the combined  $\Upsilon(1S, 2S)$  data sample. The significance of the excess, assuming that it has the same origin as the  $P_{c\bar{c}s}(4459)^0$  candidate [6] is  $3.3\sigma$ , including systematic uncertainties. The branching fraction for  $P_{c\bar{c}s}(4459)^0$  production in inclusive  $\Upsilon(1S, 2S)$  decay are determined to be  $\mathcal{B}[\Upsilon(1S) \rightarrow P_{c\bar{c}s}(4459)^0/\bar{P}_{c\bar{c}s}(4459)^0 + anything] = (3.5 \pm 2.0 \pm 0.2) \times 10^{-6}$  and  $\mathcal{B}[\Upsilon(2S) \rightarrow P_{c\bar{c}s}(4459)^0/\bar{P}_{c\bar{c}s}(4459)^0 + anything] = (2.9 \pm 1.7 \pm 0.4) \times 10^{-6}$ . The mass and width of  $P_{c\bar{c}s}(4459)^0$  are measured to be  $(4471.7 \pm 4.8 \pm 0.6)$  MeV/ $c^2$  and  $(21.9 \pm 13.1 \pm$

2.7) MeV, respectively. We determine upper limits on  $P_{c\bar{c}s}(4338)^0$  productions in the  $\Upsilon(1S, 2S)$  inclusive decays to be  $\mathcal{B}[\Upsilon(1S) \rightarrow P_{c\bar{c}s}(4338)^0/\bar{P}_{c\bar{c}s}(4338)^0 + \text{anything}] \cdot \mathcal{B}(P_{c\bar{c}s}(4338)^0 \rightarrow J/\psi\Lambda) < 1.8 \times 10^{-6}$  and  $\mathcal{B}[\Upsilon(2S) \rightarrow P_{c\bar{c}s}(4338)^0/\bar{P}_{c\bar{c}s}(4338)^0] + \text{anything}] \cdot \mathcal{B}(P_{c\bar{c}s}(4338)^0 \rightarrow J/\psi\Lambda) < 1.6 \times 10^{-6}$ .

This work, based on data collected using the Belle II detector, which was built and commissioned prior to March 2019, was supported by Higher Education and Science Committee of the Republic of Armenia Grant No. 23LCG-1C011; Australian Research Council and Research Grants No. DP200101792, No. DP210101900, No. DP210102831, No. DE220100462, No. LE210100098, and No. LE230100085; Austrian Federal Ministry of Education, Science and Research, Austrian Science Fund (FWF) Grants DOI: 10.55776/P34529, DOI: 10.55776/J4731, DOI: 10.55776/J4625, DOI: 10.55776/M3153, and DOI: 10.55776/PAT1836324, and Horizon 2020 ERC Starting Grant No. 947006 “InterLeptons”; Natural Sciences and Engineering Research Council of Canada, Compute Canada and CANARIE; National Key R&D Program of China under Contract No. 2022YFA1601903, National Natural Science Foundation of China and Research Grants No. 11575017, No. 11761141009, No. 11705209, No. 11975076, No. 12135005, No. 12150004, No. 12161141008, No. 12475093, and No. 12175041, and Shandong Provincial Natural Science Foundation Project ZR2022JQ02; the Czech Science Foundation Grant No. 22-18469S and Charles University Grant Agency project No. 246122; European Research Council, Seventh Framework PIEF-GA-2013-622527, Horizon 2020 ERC-Advanced Grants No. 267104 and No. 884719, Horizon 2020 ERC-Consolidator Grant No. 819127, Horizon 2020 Marie Skłodowska-Curie Grant Agreement No. 700525 “NIOBE” and No. 101026516, and Horizon 2020 Marie Skłodowska-Curie RISE project JENNIFER2 Grant Agreement No. 822070 (European grants); L’Institut National de Physique Nucléaire et de Physique des Particules (IN2P3) du CNRS and L’Agence Nationale de la Recherche (ANR) under Grant No. ANR-21-CE31-0009 (France); BMBF, DFG, HGF, MPG, and AvH Foundation (Germany); Department of Atomic Energy under Project Identification No. RTI 4002, Department of Science and Technology, and UPES SEED funding programs No. UPES/R&D-SEED-INFRA/17052023/01 and No. UPES/R&D-SOE/20062022/06 (India); Israel Science Foundation Grant No. 2476/17, U.S.-Israel Binational Science Foundation Grant No. 2016113, and Israel Ministry of Science Grant No. 3-16543; Istituto Nazionale di Fisica Nucleare and the Research Grants BELLE2, and the ICSC – Centro Nazionale di Ricerca in High Performance Computing, Big Data and Quantum Computing, funded by European Union – NextGenerationEU; Japan Society for the Promotion of Science, Grant-in-Aid for Scientific

Research Grants No. 16H03968, No. 16H03993, No. 16H06492, No. 16K05323, No. 17H01133, No. 17H05405, No. 18K03621, No. 18H03710, No. 18H05226, No. 19H00682, No. 20H05850, No. 20H05858, No. 22H00144, No. 22K14056, No. 22K21347, No. 23H05433, No. 26220706, and No. 26400255, and the Ministry of Education, Culture, Sports, Science, and Technology (MEXT) of Japan; National Research Foundation (NRF) of Korea Grants No. 2016R1-D1A1B-02012900, No. 2018R1-A6A1A-06024970, No. 2021R1-A6A1A-03043957, No. 2021R1-F1A-1060423, No. 2021R1-F1A-1064008, No. 2022R1-A2C-1003993, No. 2022R1-A2C-1092335, No. RS-2023-00208693, No. RS-2024-00354342 and No. RS-2022-00197659, Radiation Science Research Institute, Foreign Large-Size Research Facility Application Supporting project, the Global Science Experimental Data Hub Center, the Korea Institute of Science and Technology Information (K24L2M1C4) and KREONET/GLORIAD; Universiti Malaya RU grant, Akademi Sains Malaysia, and Ministry of Education Malaysia; Frontiers of Science Program Contracts No. FOINS-296, No. CB-221329, No. CB-236394, No. CB-254409, and No. CB-180023, and SEP-CINVESTAV Research Grant No. 237 (Mexico); the Polish Ministry of Science and Higher Education and the National Science Center; the Ministry of Science and Higher Education of the Russian Federation and the HSE University Basic Research Program, Moscow; University of Tabuk Research Grants No. S-0256-1438 and No. S-0280-1439 (Saudi Arabia), and Researchers Supporting Project number (RSPD2025R873), King Saud University, Riyadh, Saudi Arabia; Slovenian Research Agency and Research Grants No. J1-9124 and No. P1-0135; Agencia Estatal de Investigación, Spain Grant No. RYC2020-029875-I and Generalitat Valenciana, Spain Grant No. CIDEAGENT/2018/020; The Knut and Alice Wallenberg Foundation (Sweden), Contracts No. 2021.0174 and No. 2021.0299; National Science and Technology Council, and Ministry of Education (Taiwan); Thailand Center of Excellence in Physics; TUBITAK ULAKBIM (Turkey); National Research Foundation of Ukraine, Project No. 2020.02/0257, and Ministry of Education and Science of Ukraine; the U.S. National Science Foundation and Research Grants No. PHY-1913789 and No. PHY-2111604, and the U.S. Department of Energy and Research Awards No. DE-AC06-76RLO1830, No. DE-SC0007983, No. DE-SC0009824, No. DE-SC0009973, No. DE-SC0010007, No. DE-SC0010073, No. DE-SC0010118, No. DE-SC0010504, No. DE-SC0011784, No. DE-SC0012704, No. DE-SC0019230, No. DE-SC0021274, No. DE-SC0021616, No. DE-SC0022350, No. DE-SC0023470; and the Vietnam Academy of Science and Technology (VAST) under Grants No. NVCC.05.12/22-23 and No. DL0000.02/24-25.

These acknowledgements are not to be interpreted as an endorsement of any statement made by any of our institutes, funding agencies, governments, or their representatives.

We thank the SuperKEKB team for delivering high-luminosity collisions; the KEK cryogenics group for the efficient operation of the detector solenoid magnet and IBelle on site; the KEK Computer Research Center for on-site computing support; the NII for SINET6 network support; and the raw-data centers hosted by BNL, DESY, GridKa, IN2P3, INFN, and the University of Victoria.

- 
- [1] M. Gell-Mann, Phys. Lett. **8**, 214 (1964).  
 [2] G. Zweig, Report No. CERN-TH-401 (1964).  
 [3] R. Aaij *et al.* (LHCb Collaboration), Phys. Rev. Lett. **115**, 072001 (2015).  
 [4] R. Aaij *et al.* (LHCb Collaboration), Phys. Rev. Lett. **122**, 222001 (2019).  
 [5] Z. G. Wang, Int. J. Mod. Phys. A **36** (2021) 2150071.  
 [6] R. Aaij *et al.* (LHCb Collaboration), Sci. Bull. **66**, 1278 (2021).  
 [7] R. Aaij *et al.* (LHCb Collaboration), Phys. Rev. Lett. **131**, 031901 (2023).  
 [8] A. Esposito, A. Pilloni, and A. D. Polosa, Phys. Rep. **668**, 1 (2017).  
 [9] J.-M. Richard, Few Body Syst. **57**, 1185 (2016).  
 [10] X.-K. Dong, F.-K. Guo, and B.-S. Zou, Progr. Phys. **41**, 65 (2021).  
 [11] F.-K. Guo, C. Hanhart, Ulf-G. Meißner, Q. Wang, Q. Zhao, and B.-S. Zou, Rev. Mod. Phys. **90**, 015004 (2018); **94** 029901(E) (2022).  
 [12] F.-K. Guo, X.-H. Liu, and S. Sakai, Prog. Part. Nucl. Phys. **112**, 103757 (2020).  
 [13] J. L. Rosner, Phys. Rev. D **69**, 094014 (2004).  
 [14] C. E. Carlson, J. R. Hiller and R. J. Holt, Annu. Rev. Nucl. Part. Sci. **47**, 395 (1997).  
 [15] D. M. Asner *et al.* (CLEO Collaboration), Phys. Rev. D **75**, 012009 (2007).  
 [16] H. Albrecht *et al.* (ARGUS Collaboration), Phys. Lett. B **236**, 102 (1990).  
 [17] J. P. Lees *et al.* (BABAR Collaboration), Phys. Rev. D **89**, 111102(R) (2014).  
 [18] X. Dong *et al.* (Belle Collaboration), arXiv:2403.04340.  
 [19] S. Kurokawa and E. Kikutani, Nucl. Instrum. Methods Phys. Res., Sect. A **499**, 1 (2003).  
 [20] T. Abe *et al.*, Prog. Theor. Exp. Phys. **2013**, 03A001 (2013).  
 [21] A. Abashian *et al.* (Belle Collaboration), Nucl. Instrum. Methods A **479**, 117 (2002); also see detector section in J. Brodzicka *et al.*, Prog. Theor. Exp. Phys. **2012**, 04D001 (2012).  
 [22] C. P. Shen *et al.* (Belle Collaboration), Phys. Rev. D **82**, 051504 (2010).  
 [23] X. L. Wang *et al.* (Belle Collaboration), Phys. Rev. D **84**, 071107 (2011).  
 [24] D. J. Lange, Nucl. Instrum. Methods A **462**, 152 (2001).  
 [25] T. Sjostrand, S. Mrenna and P. Z. Skands, JHEP **05**, 026 (2006).  
 [26] R. Brun *et al.*, CERN Report No. DD/EE/84-1, 1984.  
 [27] T. Kuhr *et al.* (Belle II Collaboration), Comput. Softw. Big Sci. **3**, 1 (2019).  
 [28] M. Gelb, T. Keck, M. Prim, *et al.*, Comput. Softw. Big Sci. **2**, 9 (2018).  
 [29] E. Nakano, Nucl. Instrum. Methods A **494**, 402 (2002).  
 [30] K. Hanagaki *et al.*, Nucl. Instrum. Methods A **485**, 490 (2002).  
 [31] A. Abashian *et al.*, Nucl. Instrum. Methods A **491**, 69 (2002).  
 [32] M. Feindt and U. Kerzel, Nucl. Instrum. Methods A **559**, 190 (2006).  
 [33] S. Navas *et al.* (Particle Data Group), Phys. Rev. D **110**, 030001 (2024).  
 [34] S. Actis. *et al.*, Eur. Phys. J. C **66**, 585 (2010).  
 [35] X. K. Dong, X. H. Mo, P. Wang, and C. Z. Yuan, Chin. Phys. C **44**, 083001 (2020).